Combining low-temperature thermochronology with 3-D probabilistic kinematic modeling of the Bavarian Subalpine Molasse

Sofia Brisson[1,2*], Denise Degen[2], Florian Wellmann[2,3], and Christoph von Hagke[1]

[1]Department of Environment and Biodiversity, Paris Lodron University Salzburg, Austria.

[2]Department of Computational Geoscience, Geothermics and Reservoir Geophysics, RWTH Aachen University, Germany.

[3]Fraunhofer Research Institution for Energy Infrastructures and Geothermal Systems (IEG), Germany.

*Corresponding author: Sofia Brisson (brisson@cgre.rwth-aachen.de)

Key Points:

- An accurate interpretation of the Alps' time-temperature evolution requires considering geometric and kinematic uncertainties.
- Modeling parameters can be refined using geological inversion employing Markov chain Monte Carlo sampling and auxiliary thermochronology data.
- Low-temperature thermochronological data may not be informative enough to reduce modeling parameter uncertainties.

Abstract

To understand the exhumation history of the Alpine foreland, it is important to accurately reconstruct its time-temperature evolution. This is often done employing thermokinematic models. One problem of many current approaches is that they are limited to 2-D and do not consider structural or kinematic uncertainties. In this work, we combine 3-D kinematic forward modeling with a systematic random sampling approach to automatically generate an ensemble of kinematic models in the range of assigned geometric uncertainties. Using Markov chain Monte Carlo, each randomly generated model will be assessed in regards to how well they fit the available thermochronology data. This is done to obtain an updated set of modeling parameters with reduced uncertainty. The resulting, more robust model can then be used to re-interpret the thermochronological data and find alternative drivers of cooling for certain samples.We apply this approach to a simple synthetic model to test the methodology, and then to the Eastern Alps triangle zone in the Bavarian Subalpine Molasse. Results show that it is possible to translate low-temperature thermochronology data into a likelihood function to obtain a 3-D kinematic model with updated, more probable parameters. The thermochronological data by itself, however, may not be informative enough to reduce the parameter uncertainty. The method is useful, however, to study alternative mechanisms of exhumation for the thermochronological samples that are not respected by the modeling, even when uncertainty is considered.

Plain language summary

Understanding how the Alps have changed over time requires accurately tracking its temperature history. Current methods often fall short because they are limited to 2-D representations and do not consider uncertainties. Low-temperature thermochronology can be useful to study the thermal and tectonic history of the upper few kilometers of the Earth's crust. Kinematic models, on the other hand, serve to describe the tectonic and structural evolution. However, it is important to consider more than one possible structural evolution. In this work, we use thermochronological data as a constraint to decide which randomly generated kinematic model is more probable. It is important to study whether the thermochronological data can act as a good-enough constraint, and whether this method can allow us to discern different factors acting in the Alpine tectonic evolution.

1 Introduction

Building accurate 3-D kinematic models is important to interpret and validate cooling ages from thermochronological data. These are important and widely used to study the tectono-thermal and exhumation history of the uppermost crust. However, the interpretation of exhumation in mountain belts on the basis of thermochronologic data can yield precise but not necessarily accurate solutions due to uncertainties in both geometric and kinematic models, in addition to methodological uncertainties associated with thermochronological data.

Though limited studies exist that have recognized this and include geometric uncertainty in their models (Brisson et al., 2023; Evans et al., 2015; Parks and McQuarrie, 2019), a full

assessment of the influence of geometric and especially kinematic uncertainty on the interpretation of thermochronological data is yet missing. This can be problematic, as predicting the deep structure of the subsurface is uncertain due to the lack of surface and subsurface data. Furthermore, the geometric models are subject to interpretation bias (Bond, 2015; Bond et al., 2012), and may suffer from adopting idealized models (Butler et al., 2018). Shortening estimates and structural models may vary substantially when taking uncertainty into account (e.g. Judge and Allmendinger, 2011). For example, the same shortening rate acting on faults of uncertain dip can affect the estimated rates of exhumation. Furthermore, different structures may be active at different times, but result in similar exhumation scenarios (Figure 1a). This means that geometric or kinematic uncertainties do not necessarily manifest themselves in a difference in cooling ages. Thus, these geometric and kinematic uncertainties should manifest themselves as errors in subsequent studies, namely in the construction of thermokinematic models, which may result in an inaccurate interpretation of the tectonic evolution of an orogen.

The area of the foreland fold-thrust belt of the Alps, i.e. the Subalpine Molasse, is particularly suited to resolve large-scale dynamics of the orogen, as it links the Alps with its foreland. Despite research in this area ongoing for many years (e.g. Ganss and Schmidt-Thomé, 1952; Mock et al., 2020; Ortner et al., 2015, 2023; von Hagke et al., 2014), the structural variability and internal geometry is still not well understood, and different interpretations of data are possible (Frings et al., 2023; von Hagke and Malz, 2018). Similarly, relative timing of deformation and associated strain partitioning across different faults has been dated in some parts of the fold-thrust belt (Cederbom et al., 2004; Ortner et al., 2015; von Hagke et al., 2012, 2014), while in other regions it is not yet well known. Different conceptual models are possible because field evidence of structures is limited due to vegetation cover and anthropogenic influence on the landscape, while seismic data is not available everywhere and sometimes lacks borehole control. Omitting the uncertainties of structural interpretations can make it difficult to evaluate thermokinematic models, and thus eventually to draw conclusions about the underlying processes driving mountain building.

In this work, we explore the influence of structural uncertainty on exhumation models. For this, we generated a stochastic ensemble of 3-D kinematic models where fault slip and geometry of selected faults are varied in each run. We use Markov chain Monte Carlo (MCMC) to compare the models to available thermochronological data and to characterize the posterior uncertainty. Likely models can then be determined on the basis of whether they provide suitable predictions of the observed thermochronological data (Figure 1b). The method aims to reduce the uncertainty of the kinematic model and to obtain more accurate exhumation estimates that account for geometric and kinematic uncertainties. Because of the complex nature of our kinematic model, the MCMC is tested on two benchmark studies before being applied to the Subalpine Molasse. First, we develop a very simple model to visualize the effects of the sampling and to test different convergence diagnostics. Then, we use the complex model with synthetic, known, target parameters, to show that the method works for real world scenarios, and that limitations can arise from the nature and quality of the data.

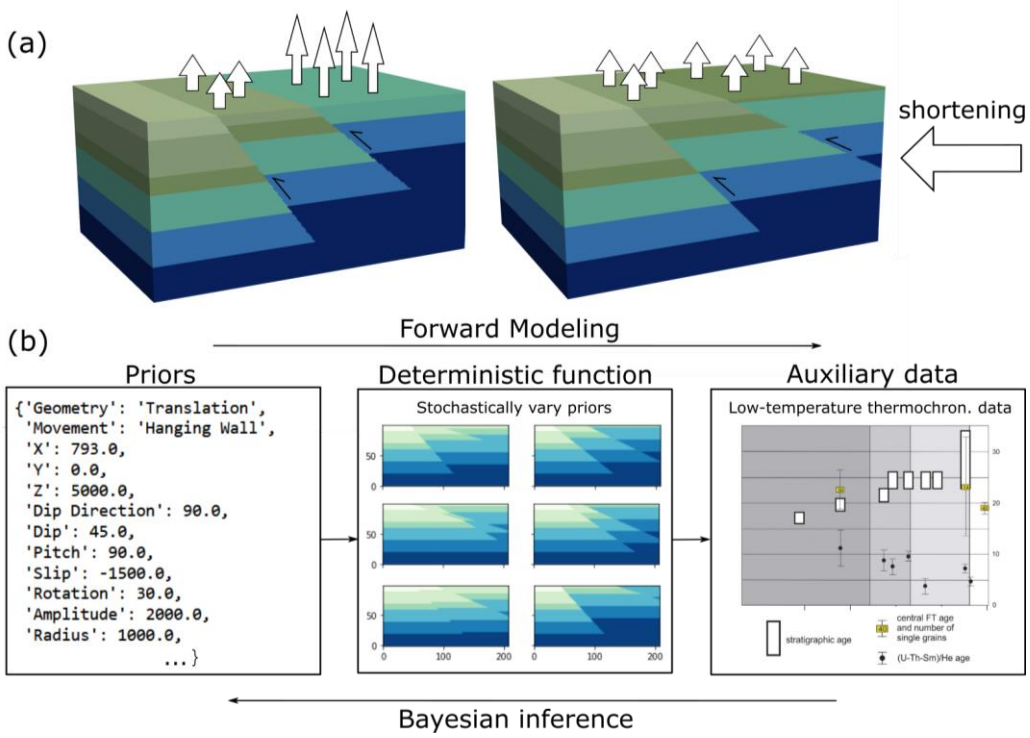

Figure 1. a) Two possible fault configurations for a single model. Applying the same shortening leads to different exhumation rates. b) Shows a basic Bayesian network containing three nodes (priors, the deterministic function represented by Noddy, and the likelihood given by the additional auxiliary data).

2 Geological setting

The area we focus on can be found in the European Alps southeast of Lake Constance. It is part of the foreland basin of the Alps - the Molasse basin, which formed in the Neogene during the later stages of the Alpine orogeny, as a result of the flexural bending of the European plate (Pfiffner, 1986). In the Molasse basin, three distinct parts are recognized: a) the mostly undeformed Plateau Molasse between the Subalpine Molasse and the external Jura fold-thrust belt, b) the Foreland Molasse, i.e., the undeformed basin east of the Jura fold-thrust belt (Ortner et al., 2015, 2023), and c) the Subalpine Molasse. The latter consists of several south-dipping thrust sheets, though north-dipping backthrusts forming its characteristic triangle zone can be found in some regions, including the study area (Ortner et al., 2015; Schuller et al., 2015). The Subalpine Molasse developed starting from 35 Ma, when foreland sediments were incorporated into the Alpine wedge (Homewood et al., 1986; Kempf et al., 1999).

In the late Miocene, the deformation of the Jura fold-thrust belt started to the west of Zurich, where Permian and Triassic evaporites acted as a decollement, transforming the Plateau Molasse into a wedge-top basin (e.g., Bolliger et al., 1993; Burkhard and Sommaruga, 1998; Laubscher, 1961). Thus, in the western foreland, strain is partitioned between the external Jura fold-thrust belt and the Subalpine Molasse. Also in the west, studies show that the Subalpine Molasse has been active since shortly after deposition of foreland basin sediments (Cederbom et al., 2004; von Hagke et al., 2012). This would indicate additional drivers for basin exhumation

other than plate convergence (Cederbom et al., 2004, 2011; Mock et al., 2020; von Hagke et al., 2012). On the other hand, between Lake Constance and Munich, the Subalpine Molasse accommodates all shortening, and thermochronological data south of Lake Constance corroborate a late-stage reactivation of internal thrusts of the foreland fold-thrust belt (von Hagke et al., 2014). East of Lake Constance, preliminary results indicate little exhumation of the external structures. Additionally to the east, the Subalpine Molasse is partly absent or overridden by late thrusting within the Flysch units (Hinsch, 2013).

Within the Molasse sediments, two regressive coarsening-upward sequences can be distinguished (Homewood et al., 1986; Kuhlemann and Kempf, 2002). These include the Lower Marine Molasse (UMM), the Lower Freshwater Molasse (USM), the Upper Marine Molasse (OMM), and the Upper Freshwater Molasse (OSM). South of the basal Alpine thrust in the study area, we can also find units of the Rhenodanubian Flysch (RDF), product of the closure of the Penninic ocean in the Paleogene (Trümpy, 1960), and Helvetic units, accreted to the Alpine wedge during the Eocene-Oligocene boundary (Pfiffner, 1986).

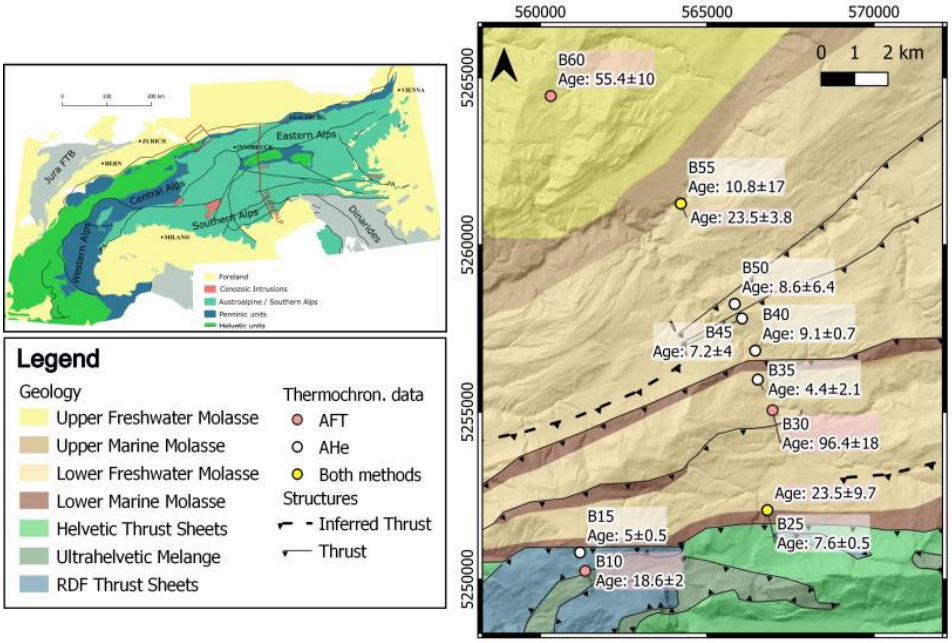

Figure 2. Tectonic map of the modeled area showing the position of the low-temperature thermochronological samples from von Hagke et al., 2014.

3 Methods

3.1 Kinematic Modeling

Constraining exhumation histories from thermal histories using low-temperature thermochronology can be uncertain (Reiners et al., 2005). Even without considering the inherent uncertainty in assuming paleogeothermal gradients, the exhumation history from the thermochronological data alone can only be roughly estimated. Kinematic reconstructions are important tools to reduce the uncertainty in interpretations, and combined with thermochronological data can yield more accurate exhumation values. Thermochronological data

has been combined with kinematic modeling in past studies in order to validate existing, well-constrained cross sections (e.g. Eizenhöfer et al., 2023; Erdős et al., 2014; Parks and McQuarrie, 2019). However, these studies are limited to 2D, and more importantly, consider only one or a limited range of possible kinematic and geometric scenarios. That is why, instead of a deterministic kinematic reconstruction based on a present-day geometric model, we generate probabilistic 3-D kinematic forward models. In these forward models, we consider major kinematic events and their properties. We omit local features, often included in high-resolution deterministic reconstructions, as long as they are not significant to the observed setting in the range of uncertainties. Transitioning from a high-resolution deterministic reconstruction to a probabilistic forward model of lower resolution is also motivated by the realization that, due to the diffusive character of heat transport, the temperature field is less sensitive to small geometric variations. And, more importantly, it would allow us to consider uncertainties in the kinematic forward models.

We built the initial kinematic models using Noddy (Jessell, 1981; Jessell and Valenta, 1996), a 3-D forward geomodeling software. Despite its limitations in reproducing complex geological features, we use Noddy because the focus of this study is to illustrate the potential of probabilistic uncertainty quantification, and therefore complexity is not the highest priority. Relevant features can still be produced, exhibiting a comparable level of topological complexity (Thiele et al., 2016). Furthermore, with Noddy's python wrapper pynoddy (Wellmann et al., 2016), it is possible to stochastically perturb the model parameters to simulate uncertainty. While Noddy was initially meant for creating simple models for teaching purposes, it has also been used for studying concepts such as geological topology (Thiele et al., 2016), and machine learning techniques (Guo et al., 2021). In addition, it has been used for geophysical inversion (Pollack et al., 2020).

Models can be constructed by combining different user-defined events (e.g. faulting, folding, tilting) upon a designated stratigraphic pile. These events are interpreted by Noddy as a sequence of kinematic operations. This process ensures that the resulting model is balanced.

3.2 Assigning uncertainty and local sensitivity study

All geological data is associated with uncertainty. In this work, we cover uncertainties pertaining to error, bias, or imprecisions (i.e., Type 1 errors as defined by Mann, 1993 and later adapted for geological modeling by Wellmann et al., 2010), which are present in any type of raw data. These types of uncertainties, as opposed to uncertainties that result from lacking knowledge, are handled with geostatistical methods.

The next step is thus assigning uncertainty through probability density functions (PDFs) to the model inputs. These include kinematic parameters such as fault slip and slip azimuth, and geometric parameters like position, fault dip, fault curvature amplitude and dip direction. Geological models of this region are largely built upon seismic lines, as boreholes are scarce and outcrops are often limited due to vegetation. This means that we expect that any model built from this data will be uncertain (von Hagke and Malz, 2018).

For simplicity, not all modeling parameters were varied simultaneously. In the synthetic model, the exhumation only depends on the fault dip and the fault slip, because the faults are planar and exhumation can thus be calculated through trigonometry. Thus, only these parameters were varied. In the case study, faults exhibit more complex geometries, so we carried out a sensitivity analysis to estimate the expected changes in exhumation rate caused by the different parameters (Figure 3). We ran 50 simulations where we took turns varying each parameter in regular intervals of 200 m or 2° while keeping the rest of the parameters fixed, and calculated the resulting exhumation for each new parameter value. For comparison, the relative percentage change of the exhumation was calculated and is shown in Figure 3a. The scenario analysis showed that many parameters exert control over the exhumation, however, not all of these behave in the expected way. For example, varying the slip direction can change thrust faults into strike-slip faults. Varying dip direction or the position in the x-direction of the fault, on the other hand, can result in the sample ending up in a different tectonic slice. Furthermore, changing the dip of curved faults in Noddy will pivot the entire fault in a non-realistic way. So even though the effect on the exhumation is large, it may not be geologically correct. After thorough examination, we chose to vary the fault slip and the fault depth (Z).

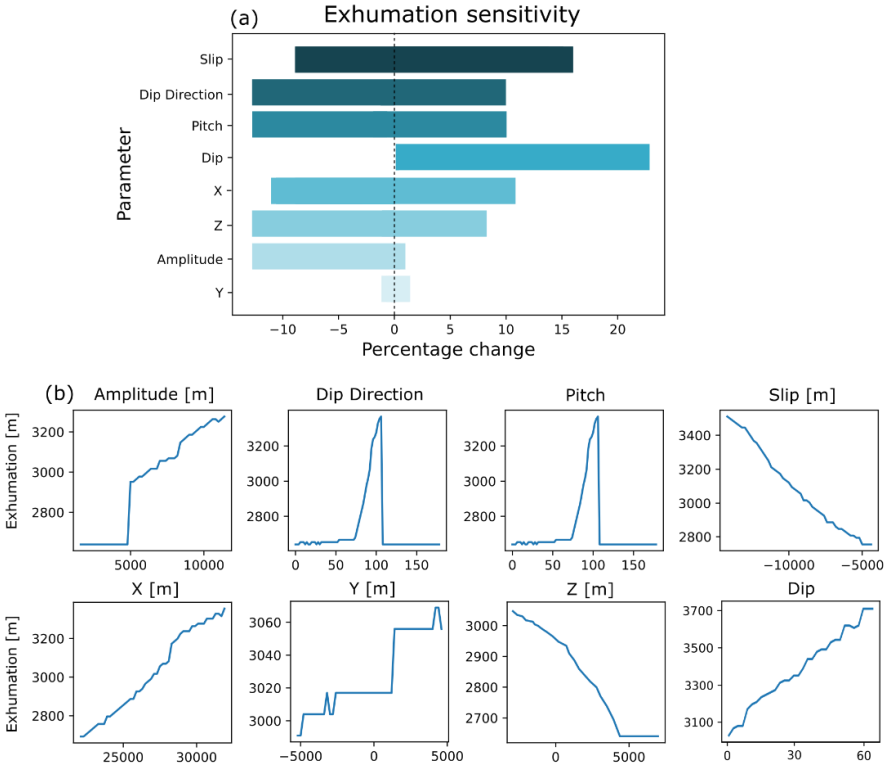

Figure 3. (a) Tornado plot showing the percentage change of the calculated exhumation when each parameter is varied by a regular amount while keeping all other parameters constant. (b) Plots showing the exhumation response to the change of each parameter.

The choice of suitable probability density functions for these parameters is described in more detail below where the model setups are detailed. For all cases, we use the initial values the mean and the assigned uncertainty as the standard deviation to define the PDFs.

Next, we use our initial model as a base to simulate new input data sets from the assigned PDFs. For each stochastic run, we compare the current model to its pre-deformation state (regional tilting was included as pre-deformation). Assuming steady state topography we can calculate the exhumation, here referring to vertical movement of the sample as its difference in position before and after the deformation events (Figure 4). For this, it is necessary to recompute the model after disturbing the parameters in each run, so that the new sample positions can be extracted from the pynoddy lithology block (i.e. a voxel model with an assigned lithology in each cell).

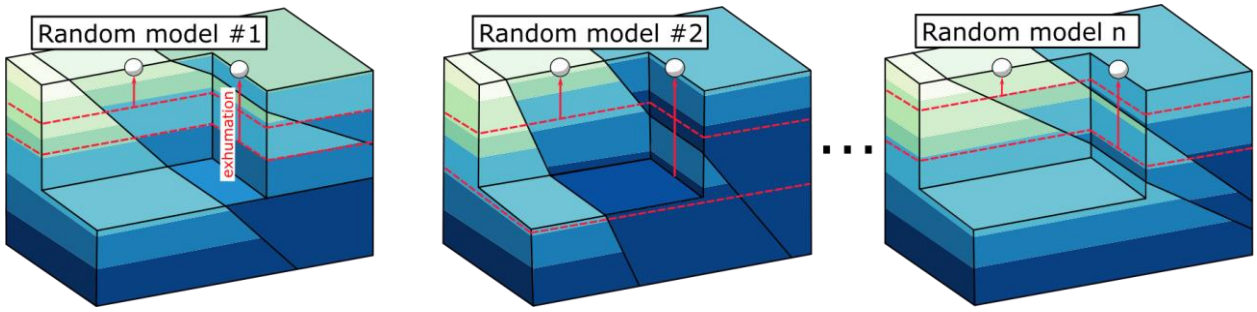

Figure 4. Three randomly generated models, with the original, non-deformed stratigraphy marked as red dashed lines. The exhumation is calculated as the vertical distance between the position of the rock before and after the deformation events (whole red lines).

3.3 Thermochronological methods and data

Apatite (U-Th-Sm)/He (AHe) and apatite fission track (AFT) dating methods are useful for tracing the tectono-thermal history of the uppermost 2 to 3 km of the crust, and are sensitive to cooling intervals between 80-40°C and 120-60°C, respectively (Carlson et al., 1999; Wolf et al., 1996). These intervals are also known as the partial retention zone (PRZ) and partial annealing zone (PAZ). If an apatite grain is subjected to reheating during burial, it will yield progressively younger cooling ages, until it is completely reset. Combining the AHe and AFT systems, which reset at different temperatures, has proven valuable in distinguishing cooling histories (Stockli, 2005). By assuming a paleogeothermal gradient, it is possible to estimate how deep the rock was buried prior to its exhumation based on its cooling age, as well as ascertain the maximum temperature attained within the basin. For a more in-depth description of the method, we refer the reader to Farley and Stockli, 2002.

We employed the available AHe and AFT data from the Bregenz region (von Hagke et al., 2014) to evaluate the methodology used in this study. von Hagke et al., 2014 describe four different structural domains bound by major faults. These are, from south to north: 1) all units south of the basal Alpine thrust, 2) limited to the north by the basal UMM thrust, 3) the triangle zone, and 4) the mostly undeformed Plateau Molasse. Samples were taken to represent each tectonic slice, and the results are summarized in Table 1.

Sample ID	Tectonic Slice	AHe system reset?	AFT system reset?	Pre-exhumation depth [km]
B10	1	-	Yes	>4.8
B15	1	Yes	-	>3.2
B25	2	Yes	Partially	3.2 >z >4.8
B30	2	-	No	<3
B35	2	Yes	-	>3.2
B40	3	Yes	-	>3.2
B45	3	Yes	-	>3.2
B50	3	Yes	-	>3.2
B55	4	Yes	Partially	3.2 >z >4.8
B60	4	-	No	<3

Table 1
Low-temperature thermochronology data from von Hagke et al., 2014. The pre-exhumation depth was estimated using existing heat flow models of the area from Frings et al. 2022 (preprint). Note that the pre-exhumation depth is better constrained when a combination of AHe and AFT is used.

3.4 Bayesian inversion

Bayesian statistics is an important tool to deal with uncertainty and updating beliefs based on both prior knowledge and observed data. Unlike the frequentist approach, which treats parameters as fixed and unknown, Bayesian statistics views them as random variables defined by a probability distribution (McElreath, 2018). Thus, the aim of Bayesian inference involves updating the prior probability $p(\theta)$ of a parameter θ (i.e., fault dip, slip) based on the use of a likelihood function $p(y|\theta)$: the probability of observing y given the parameters θ, with y being the auxiliary or observed data (in this case - thermochronological data). The likelihood function is used to compute the posterior predictive model for our parameters, $p(\theta|y)$, representing the probability of parameter θ occurring given that y was observed (Stuart, 2010) (Eq. (1)).

$$p(\theta|y) = \frac{p(y|\theta)\,p(\theta)}{\int p(y|\theta)\,p(\theta)\,d\theta} \quad \text{Eq. (1)}$$

In order to resolve this equation, we follow the steps defined in Gelman et al., 2014 that outlines the inference process. First, all of the modeling parameters θ are defined and form a prior model. This prior model is subsequently conditioned to the observations through our forward deterministic operations (in this case - our kinematic Noddy models) to obtain prior predictive models. The results are evaluated against the constructed likelihood functions. We obtain an updated version of the parameters according to new observations. Also in this step, we use sampling techniques like MCMC to approximate the integral of Eq. (1), in order to obtain a solution. The final step is to evaluate the posterior predictive model by comparing the parameter kernel density distributions or by calculating the information entropy for the model ensemble (Wellmann and Regenauer-Lieb, 2012).

For a more in-depth outline about the applications of Bayesian inference in geological modeling, we refer the reader to de la Varga et al., 2015 and de la Varga and Wellmann, 2016.

3.5 MCMC

When performing random model realizations (e.g., using Monte Carlo sampling), we may end up computing models that are far from geological reality. In Monte Carlo sampling, prior uncertainties are propagated without considering any data, yielding larger margins of uncertainty and "pessimistic" predictions. By incorporating geological modeling into a Bayesian inference framework, we can incorporate additional information to update our beliefs about the prior distributions and lead towards a reduction in uncertainty.

In this work, we define a discrete likelihood function using the thermochronological data. This data gives us a range of expected pre-cooling depths based on the sample's reset status, assuming a fixed paleo-geothermal gradient. We assign a penalty to the likelihood every time an exhumation estimate falls outside the expected range, and obtain a final joint likelihood that ultimately will depend on how many of the samples were respected by the model. We incorporate this into a Metropolis-Hastings Markov chain Monte Carlo (MH MCMC) sampling approach (Metropolis et al., 1953). The Metropolis-Hastings method is the established standard version of the MCMC algorithms. In each iteration, a new realization is proposed with a new candidate probability distribution q(θ,θ'), from which new proposed parameters θ' are drawn. Similarly, the likelihood given the observed data is evaluated. An acceptance ratio is then calculated using the following equation:

$$\alpha(\theta', \theta) = \frac{p(\theta')p(y|\theta')}{p(\theta)p(y|\theta)} \quad \text{Eq. (2)}$$

The acceptance ratio is compared to a random value sampled from a uniform distribution U(0,1), to determine acceptance or rejection of the proposed model. Basically, if the likelihood of the proposed model p(y|θ') is higher than in the previous iteration p(y|θ), then the proposed model has a higher probability to be accepted. This means that there is still a possibility of accepting models of lower likelihood and vice-versa, but it guarantees a thorough inspection of the entire parameter space (Sambridge and Mosegaard, 2002).

The Eastern Alps kinematic model, as many practical problems in geology, is defined by more than 40 parameters. A problem that is commonly encountered when using MCMC is that an extremely high number of iterations is needed to sufficiently sample the entire posterior distribution space (i.e., to converge). This convergence is needed to draw the full representation of the 3-D geological model from the posterior parameter distributions. This is why we simplify the uncertainty quantification to include the variation of only 4 parameters for the synthetic model, and 6 parameters for the complex model, on the basis of the local sensitivity analysis performed in Sec. (3.2).

4 Results

4.1 Synthetic model

4.1.1 Model setup

A synthetic model is used to exemplify how the uncertainty assessment is applied to a basic 3-D geological model and to aid in providing a clearer visualization of the sampling algorithms employed. It consists of two planar thrust faults. The prior parameterization consists of two different types of uncertain parameters associated with each fault: fault slip and fault dip angle, resulting in a total of 4 model parameters. The low number of parameters and the simple geometry of the faults facilitates the calculation of exhumation. This made computing the models and studying the method very fast and straightforward. In addition, two synthetic AHe data points are created: sample A between faults 1 and 2, and sample B to the right of fault 2 (Figure 5). Sample A has not been reset, meaning that it is above the Partial Retention Zone (assuming it is at 40°C), i.e., the temperature where no influence of burial on the thermochronological age is expected. We would thus expect an exhumation value smaller than 1.3 km (assuming a paleo-geothermal gradient of 30°/km). Sample B has been reset, so we expect an exhumation greater than 2.7 km, both assuming that the cooling is exclusively driven by exhumation.

A standard deviation of 500 m is added to the fault slip and 8° to the fault dip. Though additional uncertainties could also be included (e.g. the fault position, the slip vector pitch), the synthetic model was purposefully kept simple to better visualize the effect of the uncertainties.

As mentioned, a discrete likelihood function was defined where any models that explain the sample exhumations (< 1.3 km and > 2.7 km) were assigned a likelihood of 1. If either of the samples was not respected, then the likelihood was reduced in proportion to the proximity of the estimated exhumation to the expected value. Because the thermochronological data usually only provides broad, upper-lower-limit type constraints to exhumation, it is not possible to define a continuous likelihood function.

Two simulations were carried out using the synthetic model: an initial forward uncertainty propagation using Monte Carlo sampling without additional constraints by the thermochronological samples, and a second simulation including the Bayesian inversion using the auxiliary data. Due to the simplicity of the model, the simulations are fast so three separate MCMC chains were used to ensure convergence to the same posterior distributions.

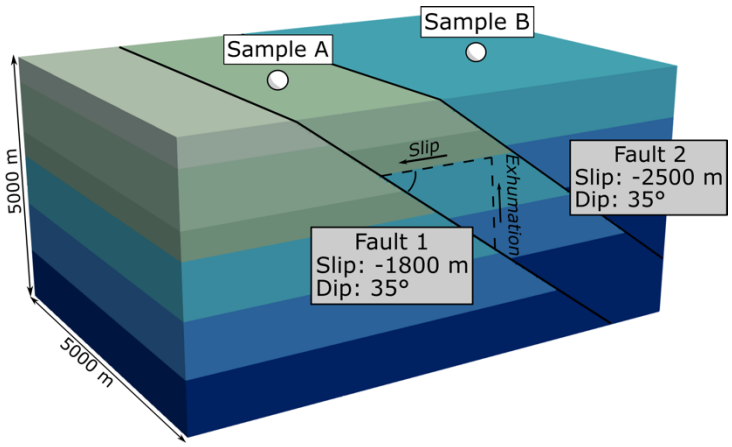

Figure 5. Synthetic model and synthetic samples. In this case, the exhumation depends solely on the fault slip and the fault dips. If we consider the exhumation as vertical movement, then it can be calculated as the cosine of the dip angle multiplied by the horizontal slip vector.

4.1.2 Result analysis

Using the starting model parameters shown in Figure 5, a total of 26551 random model iterations were executed to secure 5000 accepted models using the Metropolis-Hastings MCMC sampling algorithm. This amount of runs was chosen by using convergence diagnostics to ensure that a representative number of samples was taken. The posterior parameter analysis shows that there is an increase in the parameter means, especially for fault 2, which must account for the relatively high amount of exhumation for sample B to be respected. Additionally, comparing the joint probability distributions shows that while the prior parameters are independent with respect to one another, the posterior parameters show correlation, and a decrease in their standard deviations, as well (Figure 6a). For example, the dip of the faults show a positive correlation with their respective slips. The correlation plots can be found in the Supplementary Material.

On the other hand, the overall standard deviation of the resulting exhumation decreases for the accepted samples (Figure 6b). The rejection algorithm also ensures that it is more probable for sample A to fall above the partial retention zone and the opposite for sample B. By definition, in its exploration of the parameter space, MCMC sampling methods will occasionally accept models that do not fully obey the data or reject models that do.

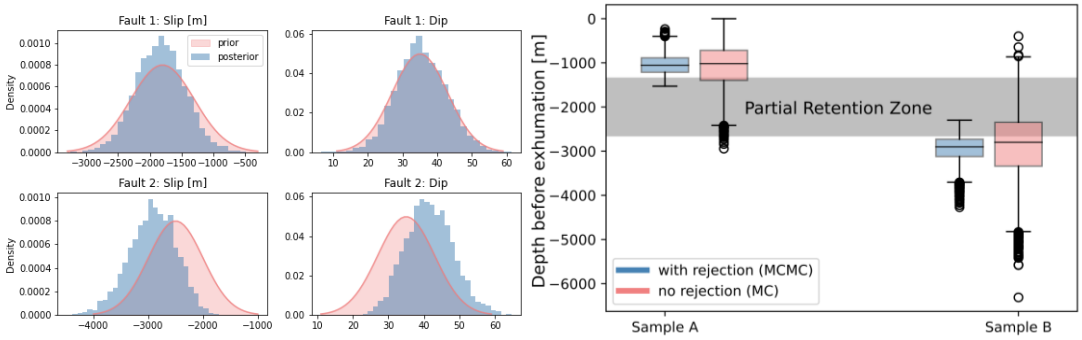

Figure 6. (a) shows the prior (red curve) and posterior (blue histogram) parameter distributions. (b) Boxplot showing the accepted model exhumation calculations (blue) after using MCMC sampling, and all model exhumation calculations (red) without rejection sampling.

We use the concept of information entropy (Wellmann and Regenauer-Lieb, 2012) to visualize the model uncertainties (Eq. (3)).

$$H(x) = \sum_{i=1}^{N} p_i(x) log\, p_i(x) \quad \text{Eq. (3)}$$

Where H is the information entropy in each cell x and normalized across the total number of cells N. An entropy value of 0 signifies that, for a random model ensemble, there is only one solution or unit known for one given voxel after many model iterations. As entropy rises, more solutions are possible with equal probability (i.e. the position of the unit is uncertain) for this voxel. We refer the reader to Wellmann and Regenauer-Lieb (2012) for further information about the use of entropy to visualize uncertainty in 3-D geomodels.

The full model average entropy was computed. For prior runs without rejection, the mean entropy for one slice of the model was 0.60, which decreased by more than 35 % to 0.38 after MCMC sampling was performed. Consequently, MCMC is useful to derive a more refined model ensemble, resulting in a more accurate representation of the likely geological configuration (Figure 7). The average final posterior model shows a notable increase in the dip and slip of fault 2.

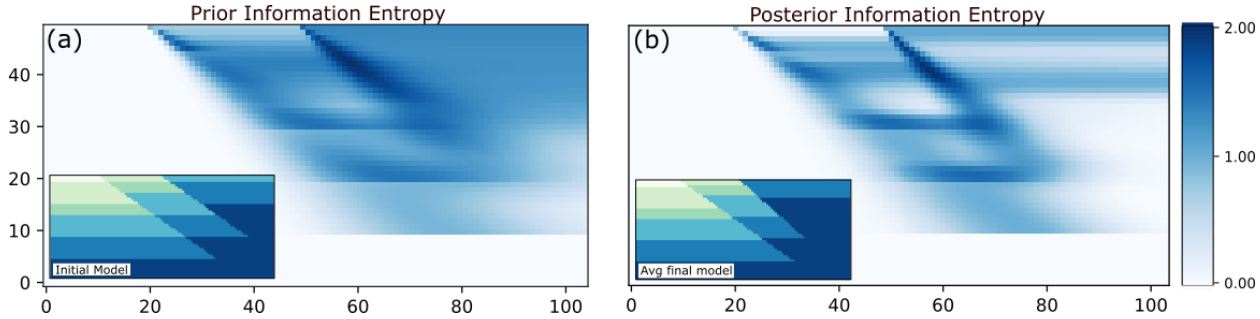

Figure 7. Information entropy of a) the prior model ensemble and b) the posterior model ensemble considering the auxiliary thermochronological information. On the bottom-left corners of the plots the updated average configurations, representing the most probable geometries, are shown.

When using MCMC methods, it is important to determine the effective number of iterations to achieve a balance between the computational time of a single run and the expected convergence. In other words, when are the accepted samples usable to estimate features of the target distribution? While convergence cannot be formally guaranteed, many methods to estimate convergence exist (see Cowles and Carlin, 1996 for a thorough review) that, while heuristic, can be combined to prove that there is no evidence against it. On one hand, we applied the method of Geweke, 1992, which quantifies how much the parameter distribution changes between the burn-in phase (or the "adjustment period" of the chain) and the end of the chain. If converged, the diagnostic should roughly follow a standard normal distribution. The synthetic model parameters are mostly within the range of 2 standard deviations (see detailed plot in the Supplementary material). Additional diagnostics such as parameter trace plots and autocorrelation plots, which check the chain's correlation with its successive lags, are available in the Supplementary Material and show no evidence against convergence. Furthermore, three chains were run

independently with consistent posterior distribution values. Based on the convergence diagnostics, a chain of 5000 iterations should be sufficiently long to estimate the target distribution space.

4.2 Case study: Bregenzarach

4.2.1 Model setup

The initial model was constructed based on published cross-sections by von Hagke et al., 2014 and Ortner et al., 2015. After the stratigraphy was defined, a series of events were combined to recreate the currently observed geometry. The faults that make up the triangle zone (duplex faults and a backthrust) were defined as the first set of structural events, followed by the two south-dipping faults that define the Salmas and Horn slices, respectively. Finally, the Alpine basal thrust lifts the Steineberg syncline (Figure 8). The Steineberg syncline is bound by a detachment that brings the Molasse sediments over the Flysch and Helvetic units (not differentiated). One limitation in the model setup is that Noddy will only operate over a predefined stratigraphy and cannot account for this type of tectonically induced lateral variations in stratigraphy. This means that when modeled, the Steineberg syncline rests over the Mesozoic and crystalline basement rocks. While we know this is not true, it can still provide at least a minimum exhumation estimate. The final model including the thermochronological samples from von Hagke et al., 2014, is shown in Figure 9.

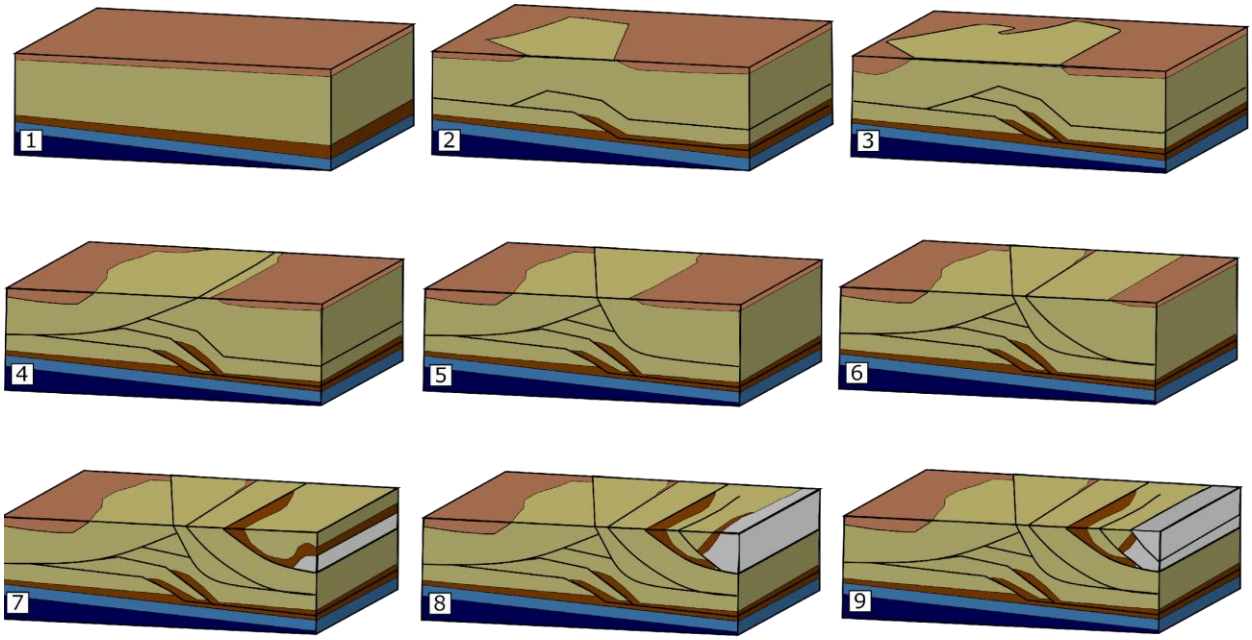

Figure 8. Series of events defined in Noddy to reach the final geometry. Note that the regional tilting of the stratigraphy is assumed here as the starting point.

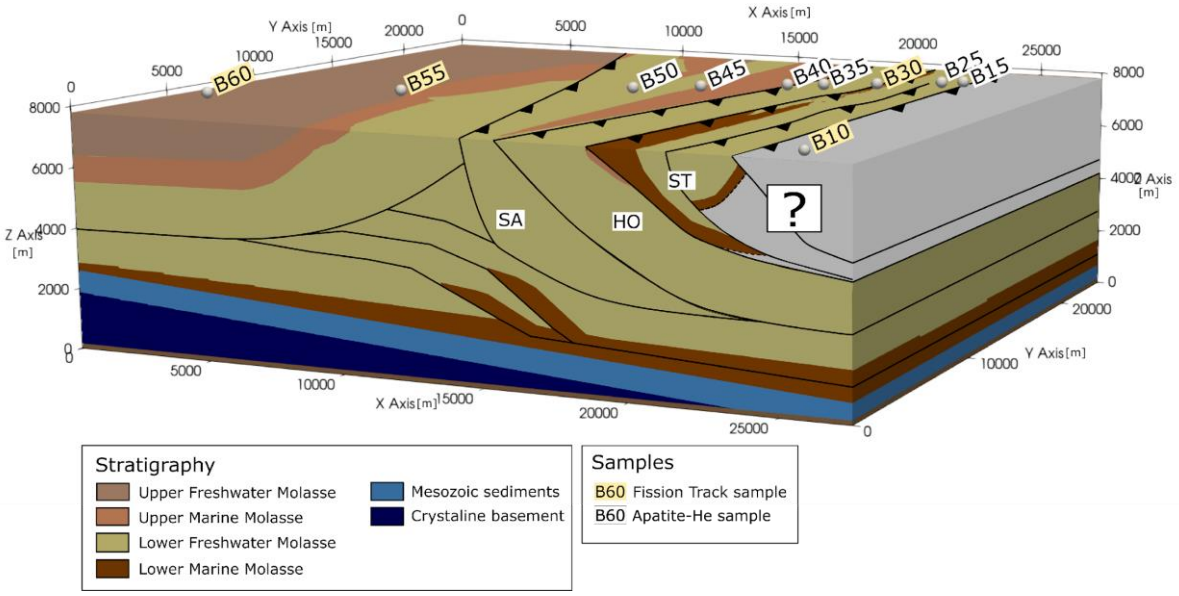

Figure 9. Final model created with Noddy and visualized using Paraview (Squillacote et al., 2007). AHe and AFT samples are from von Hagke et al., 2014. A question mark is added to the south of the Steineberg syncline because the modeling yielded an unexpected stratigraphy. Abbreviations: SA - Salmas thrust, HO - Horn thrust, ST - Steineberg syncline.

In this case, the model is defined by a large number of parameters, but after trial-and-error runs with the MCMC algorithm, only a few parameters were selected for the final stochastic modeling, to reduce the dimensionality of the problem. To decide which faults and which parameters to vary, we first computed 1000 models without rejection, and assigned a score to each random model. The score (from 1 to 10) was based on how many of the 10 thermochronological samples were respected in that particular run. Results showed that a score of 6 prevailed, followed by 4 and 5, constituting over 70% of the runs. Samples B30, B40, B50 were not respected 50% of the time, and sample B55 was respected less than 10% of the time. The rest of the samples were respected for the majority of the runs. From these results, we selected the Salmas thrust, the Horn thrust, and the thrust that brings up the Steineberg syncline (here referred to as Steineberg syncline thrust) for the inversion. These are the faults that mostly control the exhumation of samples B50, B40, and B30, respectively. Slip and depth of the faults were observed to have the greatest influence over the resulting exhumation values. This led to the selection of six parameters for the analysis. The fault depths were assigned a standard deviation of 300 m, as the geometry of the model was based purely on seismic interpretations. On the other hand, fault slips were assigned an error of 800 m. This uncertainty is enough to explore possible different configurations without straying too far from the more precise surface geology. These prior distributions were also proposed based on several trial-and-error runs to achieve a balance between the acceptance rate and convergence. Because of the slow forward modeling step, a smaller step size would have led to a very slow chain convergence.

Computing the models without the inversion was also important to determine an appropriate likelihood function. For example, samples with better constrained cooling age (i.e., possessing both an AFT and AHe age), should carry greater significance in determining the probability of rejection, than samples possessing a single cooling age. Similarly, cooling ages with big variances should result in a more lenient rejection threshold.

One additional important factor to consider is the assumptions on the paleo-geothermal gradient and its evolution through time. Ideally, we would combine the kinematic modeling in Noddy with geothermal modeling through time. Unfortunately, this has yet to be implemented in Noddy. Instead, we can use the available modeled heat flow values of the region and thermal conductivities measured in boreholes from Frings et al., 2022 (preprint), and other published heat flow estimations from vitrinite reflectance and AFT data (e.g. Mazurek et al., 2006) in order to approximate the geothermal gradient at the time of each event. These authors show that the geothermal gradient for an area directly west to our study area, in the Swiss Molasse Basin, was relatively low during the Paleogene and Neogene (15 to 25°C/km), with values increasing during the latest Neogene. Most of the samples have Miocene cooling ages that are mostly younger than their stratigraphic ages, and thus have a reset AHe system. For these cases, a geothermal gradient of 25°C/km was used to calculate the approximate pre-exhumation depth. B30 and B60, however, are both un-reset and present older ages, so a geothermal gradient of 20°C/km was used, instead.

4.2.2 Results analysis

Because of the model complexity, the amount of model runs needs to be reduced. Thus, we ran the maximum number of models possible with the available computational resources (RWTH compute cluster: 1 node, 4 cores, and 2 GB memory). By maximizing the high-performance computing resources, it was possible to run 3088 models, with 1000 accepted models within several days. On one hand, B40 and B50 had an initial pre-exhumation depth that was not deep enough to ensure full resetting of the thermochronological systems. As expected, both the Salmas and the Horn thrusts show a shift towards higher fault slips (Figure 10c). The Salmas thrust shows a minor shift upwards in depth and the opposite is true for the Horn thrust. On the other hand, the Steineberg syncline thrust shows a shift downwards in depth but the change in slip is negligible. There are small decreases in the posterior parameter standard deviations: from 300 m to around 225 m for the position at depth, and from 800 m to around 750 m for the slip (Figure 10). The average entropy for the model ensemble considering both rejected and accepted models was 0.07, which decreased to 0.06 after performing the MCMC. However, it must be pointed out that in this case entropy may not be the best description metric. In Noddy, only lithologies carry “IDs”. The modeled faults affect mostly the Lower Freshwater Molasse, so varying fault position will most likely not result in an increase in entropy.

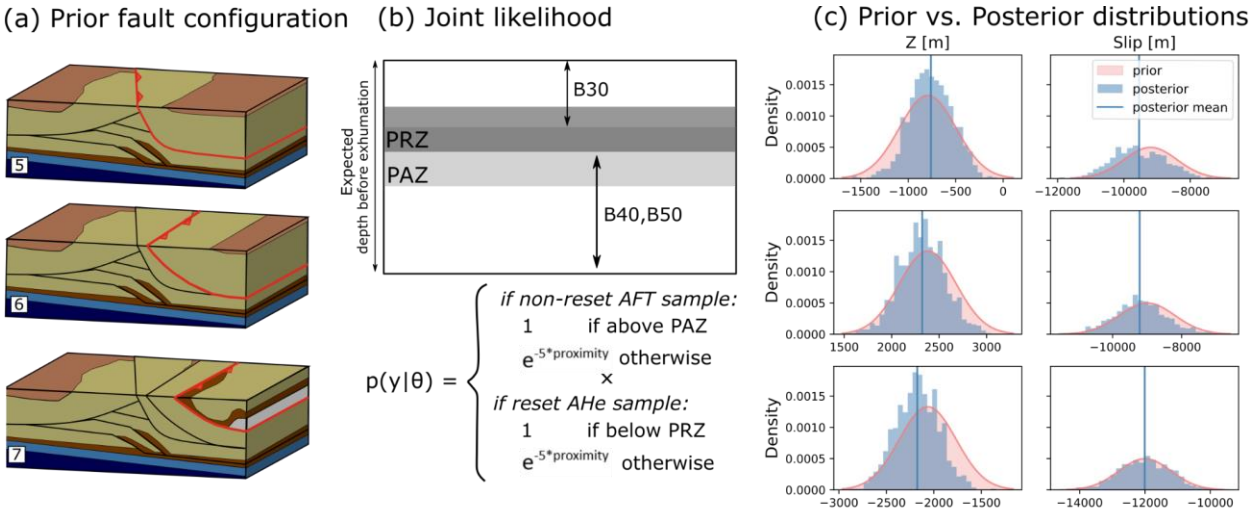

Figure 10. (a) Shows the initial fault configuration for the Salmas, Horn and Steineberg syncline thrust, respectively. (b) Schematic representation and summary of how the joint likelihood functions were constructed. (c) Resulting parameter distributions (blue histograms) after the MCMC is run compared with their priors (red curves). Abbreviations: PRZ - partial retention zone and PAZ - partial annealing zone.

Similar to the synthetic model, we checked the convergence of the MCMC chain by displaying the values of the parameters over the successive iterations in trace plots, which can be found in the Supplementary Material. The parameter trace plots exhibit stability (they fluctuate around a fixed value) and do not display any systematic trends or patterns. Geweke plots show that all parameters fall within 2 standard deviations. Autocorrelation plots show relatively low autocorrelation (not exceeding 0.2). All of the convergence diagnostics suggest that there is, again, no evidence against convergence.

In Figure 12 we divided the kinematic model into the major faulting events against a geothermal gradient. A geothermal gradient of 30°C/km was used for present-day and 20°C/km for the rest of the events. For this, the isotherms are kept undeformed under the assumption that the deformation is slow. This is supported by the modeling carried out by von Hagke et al., 2014, where most of the thermochronological samples do not require rapid exhumation. On another hand, we also assume that the cooling of the samples is purely fault driven. The final "best-fitting" model according to the MCMC was generated using the maximum a posteriori (MAP) method. This is a statistical approach which essentially finds the mode (the most probable values) of the posterior distribution parameters. It corresponds to the values of the parameters that maximize the posterior probability (Nelder and Mead, 1965). The best fitting model was then used to calculate the new, more probable, exhumation estimates for the inverted samples (shown as red triangles in Figure 11). As for the resulting exhumations, while B30 shows very small changes from the prior, B40 and B50 show a shift towards the threshold values of the likelihood functions. Particularly, B50 now lies well below the partial retention zone, and B40 can be found in its lower boundaries.

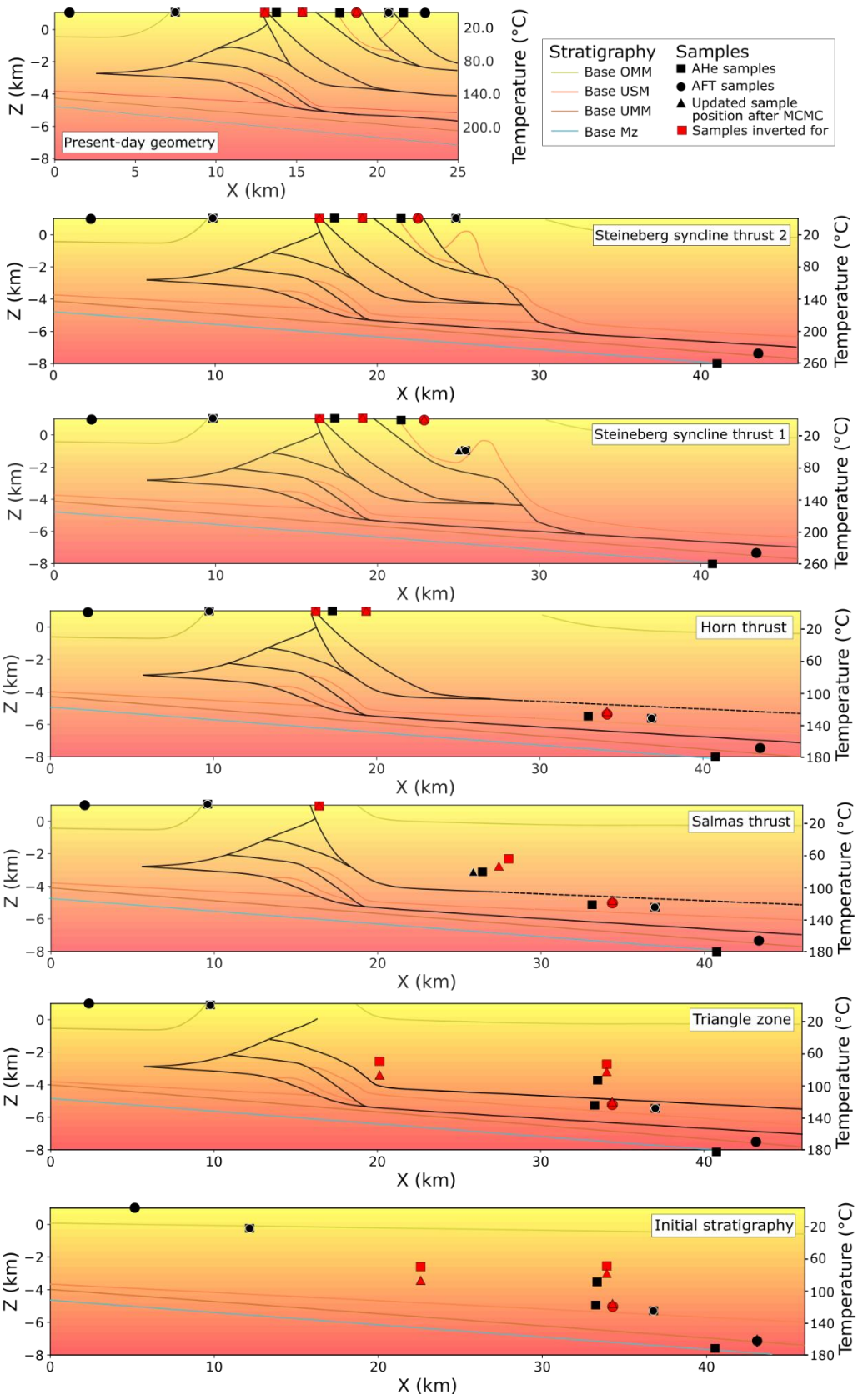
Present-day geometry
Steineberg syncline thrust 2
Steineberg syncline thrust 1
Horn thrust
Salmas thrust
Triangle zone
Initial stratigraphy
Z (km)
X (km)
Temperature (°C)
Stratigraphy
Base OMM
Base USM
Base UMM
Base Mz
Samples
AHe samples
AFT samples
Updated sample position after MCMC
Samples inverted for

Figure 11. Thermal evolution of the Bregenz triangle zone. The kinematic modeling steps were divided and combined with a very simple thermal model. The samples marked in red are the samples used for structural and kinematic parameter inversion, and the updated positions post-MCMC can be observed as triangles.

4.2.3 Test using synthetic exhumation measurements

The results do not show dramatic shifts in the posterior standard deviations. This may be because the constraints given by the thermochronological data are too broad and thus many different combinations of parameters can explain the data. That is to say, there is no unique model that can explain the data. To test out this hypothesis, we carried out a third and final experiment to ascertain that the written MCMC algorithm is functioning and to emphasize that carrying out uncertainty quantifications could still be highly beneficial when dealing with a different data set.

For this experiment, we use synthetic exhumation data that was calculated using a set of fault parameters. We then start the chain from a random initial set of parameters, and try to recover the "unknown" set of target parameters established previously using the synthetic exhumation measurements. The uncertainty used was 150 m and 400 m for the depth and slip, respectively. This time, a continuous likelihood function was defined, with the synthetic exhumation measurements defining the means of the PDFs with an assigned uncertainty of 800 m. This uncertainty was chosen to achieve the desired acceptance rate, around 30%.

We carried out 1500 models, of which around 500 were accepted. The results show that most of the parameter means have started to shift towards the known target parameters, but do not fully reach them. The MAPs were also calculated and plotted in Figure 12 together with the target and initial parameters. Only in some cases, such as the depth of the Horn thrust and the slip of the Salmas thrust, the MAPs have been shifted in the opposite direction, instead. This may be owed to the limited number of models run.

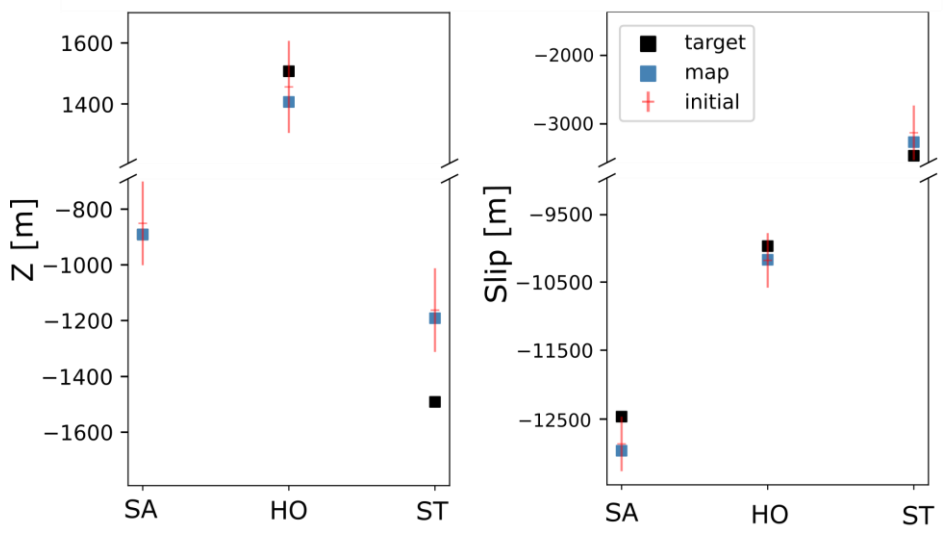

Figure 12. Plots showing a comparison between the initial parameters, the known target value of the parameters and the MAP resulting from the MCMC.

5 Discussion

The case study results and the last experiment show that the thermochronological data by itself may not act as a sufficient constraint for geometric and kinematic parameters. The overall results, however, indicate that it is feasible to consider geological modeling as a Bayesian inference problem (as has also been shown in de la Varga and Wellmann, 2016; Wellmann et al., 2018). It is possible to translate cooling ages from thermochronological data into discrete likelihood functions that serve to constrain geometric and kinematic parameters. These aspects were also successfully integrated into a probabilistic modeling framework using pynoddy, both for the synthetic and real-case studies. MCMC, as opposed to simple Monte Carlo sampling, has proven to be a powerful method not only to explore the posterior distribution space but also to obtain additional insight from the model parameters, for example how they behave in correlation to one another. The MCMC sampling has, in both experiments, yielded an updated, more probable version of the model that we started with.

The updated models can then be used to describe and analyze the thermochronological data. For example, while the prior exhumations of samples B40 and B50 were not far from the desired exhumation, samples B30 and B55, which are also not explained by the model, have extremely differing exhumation values. On one hand, the model predicts a depth before exhumation for B30 of around 6 km. B30 is a non-reset AFT sample, so it should be buried at less than 3 km, assuming a geothermal gradient of 20°C/km. Sample B35 can be found contiguous to B30, and is a completely reset AHe sample. So, there is no possible fault configuration that could explain the reset status of B30. An explanation for this could be that there is uncertainty associated with the sample position (i.e., it has been placed in the wrong tectonic slice). However, it is not easy to consider sample position uncertainty without including it as an additional model parameter into the analysis. Otherwise, a sustained geothermal gradient of around 10°C/km would be necessary to explain it in order for the sample to be not even partially reset, which would not be consistent with the other samples' status. On the other hand, sample B55 has a comparatively well-constrained cooling age because it contains at least a partially reset AFT system and a completely reset AHe system. The depth before exhumation should, in turn, also be well constrained. However, the modeling indicates only a few hundred meters of exhumation for this sample. While this could also be due to uncertainty in the sample position, another possibility is that B55 suffered reheating by a process not related to faulting.

It is also important to point out that modeling in Noddy can be challenging and comes with some limitations. Because it is a program designed for modeling simple geological scenarios, mimicking realistic structure geometries can be difficult, but possible with some simplifications. Some major limitations include a limit of around 13 km in the amount of slip that can be assigned to the faults, making it difficult to model displacement through long horizontal detachments. For example, the slip associated with the Steineberg syncline thrust did not shift at all with the MCMC. This can be because its 12 km assigned slip is already too close to Noddy's limit, and cannot recognize any slip increase. Another major limitation is simulation times, the time-limiting factor being the forward modeling step in Noddy. Keeping a high

resolution is very important and must be set at at least 100 (i.e., 1 voxel per 100 m) for the results to be significant and to fully represent the model. Furthermore, as MCMC chains are not easily parallelizable, this contributes to a big limitation in the amount of model iterations. With the current settings, running 1 model takes 5 minutes. This means that it is necessary to reduce the amount of modeling parameters used for inversion, as the number of iterations scales linearly with the amount of parameters.

The data available, on the other hand, only allows for the use of a discrete likelihood function. This can lead to non-smooth probability density functions, making it less amenable to interpolation. This may be important when making predictions or estimating probabilities for values that were not explicitly observed in the data. Additionally, using a discrete likelihood function can make the model more sensitive to specific discretization schemes used. This may lead to less robustness in the face of small changes in the data or modeling assumptions, such as a change in the assumed paleo-geothermal gradient. Because of the nature of the data, the results of the MCMC do not lead to a significant reduction in uncertainty. As shown in the final synthetic data experiment, the data seems to not be informative enough to further reduce the uncertainty in the input parameters. The use of multiple thermochronometers for a single sample, however, might provide the additional necessary constraint to obtain an uncertainty reduction.

From this result we gather that introduction of additional information does not always lead to an uncertainty reduction. Rather than a contradiction, this can mean that the prior information is not compatible with the likelihood functions (Wellmann et al., 2018). This can be seen, for example, for the initial geometry of the Steineberg syncline fault, which will never respect the thermochronological data. On the other hand, some parameter posterior means show only a slight deviation from the priors, and this can indicate that the data is already well adapted to the model.

To improve the current simulations, we plan to build a surrogate model of the forward modeling step, in order to decrease computational times (Degen et al., 2020). This will involve constructing a computationally inexpensive approximation (a surrogate model) of the complex, expensive forward simulations in Noddy. Another possible improvement could be to obtain more precise exhumation rate estimates from the cooling ages, rather than using a “threshold” exhumation. Programs like age2exhume (van der Beek and Schildgen, 2023) could be used for this purpose, though assumptions such as steady vertical uplift and topography are maintained.

Despite limitations in the computational time and model assumptions made, performing an uncertainty quantification using MCMC on kinematic models has proved useful to obtain updated modeling parameters that better explain the observed data. This is a major step forward to building a probabilistic, 3-D thermokinematic model. A thermokinematic model that accounts for uncertainties is a powerful tool to study the tectonic evolution of the area and, most importantly, helps to identify the drivers behind the exhumation.

6 Conclusions

From this study we gather the following conclusions:

- Using MCMC to perform an inversion for geometric and kinematic parameters has proven successful in providing an updated, more probable model through the introduction of auxiliary low-temperature thermochronological data.
- The simple synthetic model MCMC has performed well and led to a substantial full model entropy decrease and to a shift in parameter means and standard deviations. For the complex case study, shifts in the parameter properties were not as obvious but improvements in the predictions of the exhumations were still achieved. A separate experiment using synthetic likelihood functions has proven that, while a limitation in the number of runs does exist, the MCMC algorithm employed seems sound.
- This method could also potentially be meaningful to detect different drivers of exhumation. When the faulting in the model fails to account for the cooling age indicated by the data, it may imply the presence of an alternative cooling mechanism.
- Uncertainty quantification using MCMC, however, does not always lead to a reduction in uncertainty. Thus, low-temperature thermochronology data used in this study can only provide broad constraints and may not be informative enough to achieve a decrease in uncertainty. A combination of dating methods could be used to obtain more precise exhumation estimates.
- Though some limitations exist in applying the method to a complex, realistic geological scenario, further improvements could be made in repeating the MCMC analysis on a surrogate model to speed up computational times.

Acknowledgments

This study is part of the ThinkALPS research project funded within the Deutsche Forschungsgemeinschaft (DFG) priority program “Mountain Building in 4-D”.

Open Research

All of the code and data used for this manuscript can be found in https://github.com/s-brisson/pynoddy_exhumation.

References

Berge, T.B., Veal, S.L. (2005). Structure of the Alpine foreland. *Tectonics* 24.

Bolliger, T., Engesser, B., Weidmann, M. (1993). Première découverte de mammifères pliocènes dans le jura neuchâtelois. *Eclogae Geol. Helv* 86, 1031–1068.

Bond, C., Lunn, R., Shipton, Z., Lunn, A. (2012). What makes an expert effective at interpreting seismic images? *Geology* 40, 75–78.

Bond, C.E. (2015). Uncertainty in structural interpretation: Lessons to be learnt. Journal of Structural *Geology* 74, 185–200.

649 Brisson, S., Wellmann, F., Chudalla, N., von Harten, J., von Hagke, C. (2023). Estimating uncertainties in
650 3-D models of complex fold-and-thrust belts: A case study of the Eastern Alps triangle zone. *Applied*
651 *Computing and Geosciences*, 100115.
652 Brown, R. (1994). Apatite fission track analysis: its potential for the estimation of denudation rates and
653 implications for models of long term landscape development. *Process Models and Theoretical*
654 *Geomorphology*, 23–53.
655 Burkhard, M., Sommaruga, A. (1998). Evolution of the western Swiss Molasse basin: structural relations
656 with the Alps and the Jura belt. *Geological Society, London, Special Publications* 134, 279–298.
657 Butler, R. W., Bond, C. E., Cooper, M. A., & Watkins, H. (2018). Interpreting structural geometry in
658 fold-thrust belts: Why style matters. *Journal of Structural Geology*, *114*, 251-273.
659 Carlson, W.D., Donelick, R.A., Ketcham, R.A. (1999). Variability of apatite fission-track annealing
660 kinetics: I. Experimental results. *American Mineralogist* 84, 1213–1223.
661 Cederbom, C.E., van Der Beek, P., Schlunegger, F., Sinclair, H.D., Oncken, O. (2011). Rapid extensive
662 erosion of the North Alpine foreland basin at 5–4 Ma. *Basin Research* 23, 528–550.
663 Cederbom, C.E., Sinclair, H.D., Schlunegger, F., Rahn, M.K. (2004). Climate-induced rebound and
664 exhumation of the European Alps. *Geology* 32, 709–712.
665 Cowles, M.K., Carlin, B.P. (1996). Markov chain Monte Carlo convergence diagnostics: a comparative
666 review. *Journal of the American Statistical Association* 91, 883-904.
667 de la Varga, M., Wellmann, J.F. (2016). Structural geologic modeling as an inference problem: a
668 Bayesian perspective. *Interpretation*, 4, 1-16.
669 de la Varga, M., Wellmann, F., Murdie, R. (2015). Adding geological knowledge to improve uncertain
670 geological models: a Bayesian perspective. *Geotectonic Research*, 97, 18-20.
671 Degen, D., Veroy, K., Wellmann, F. (2020). Certified reduced basis method in geosciences. *Computat.*
672 *Geosci.*, 24, 241-259.
673 Eizenhöfer, P. R., Glotzbach, C., Kley, J., Ehlers, T. A. (2023). Thermo-kinematic evolution of the
674 Eastern European Alps along the TRANSALP transect. *Tectonics*, e2022TC007380.
675 Erdős, Z., van der Beek, P., Huismans, R. S. (2014). Evaluating balanced section restoration with
676 thermochronology data: A case study from the Central Pyrenees. *Tectonics*, *33*(5), 617-634.
677 Evans, S.L., Styron, R.H., van Soest, M.C., Hodges, K.V., Hanson, A.D. (2015). Zircon and apatite (U-
678 Th)/He evidence for Paleogene and Neogene extension in the Southern Snake Range, Nevada, USA.
679 *Tectonics* 34, 2142–2164.
680 Farley, K.A., Stockli, D.F. (2002). (U-Th)/He dating of phosphates: apatite, monazite, and xenotime.
681 *Reviews in Mineralogy and Geochemistry* 48, 559–577.
682 Frings, K. A., Luijendijk, E., Dunkl, I., Kukla, P., Villamizar-Escalante, N., Madritsch, H., von Hagke, C.
683 (2022). Unraveling the burial and exhumation history of foreland basins using the spread of apatite (U-
684 Th-Sm)/He single grain ages. *EGUsphere preprint*, *2022*, 1-51.
685 Frings, K. A., von Hagke, C., Wellmann, F., Heim, E., de la Varga, M., Ortner, H., Luijendijk, E. (2023).
686 Constraining the 3-D Geometry of Fold-Thrust Belts Using Section Balancing vs. 3-D Interpolative
687 Structural and Probabilistic Modeling. *Tektonika*, *1*, 2.
688 Ganss, O., Schmidt-Thomé, P. (1953). Die gefaltete Molasse am Alpenrand zwischen Bodensee und
689 Salzach. *Z. D. Geol. Ges*, 105, 405-495.
690 Geweke, J. (1992). Evaluating the accuracy of sampling-based approaches to the calculations of posterior
691 moments. *Bayesian Statistics* 4, 641-649.

Guo, J., Li, Y., Jessell, M.W., Giraud, J., Li, C., Wu, L., Li, F., Liu, S. (2021). 3-D geological structure inversion from noddy-generated magnetic data using deep learning methods. *Computers & Geoscience*s 149, 104701.

Hinsch, R. (2013). Laterally varying structure and kinematics of the Molasse fold and thrust belt of the Central Eastern Alps: Implications for exploration. *AAPG bulletin* 97, 1805–1831.

Homewood, P., Allen, P., Williams, G. (1986). Dynamics of the molasse basin of western Switzerland. *Foreland Basins*, 199–217.

Jessell, M.W. (1981). Noddy: an interactive map creation package. Unpublished MSc thesis, University of London.

Jessell, M.W., Valenta, R.K. (1996). Structural geophysics: Integrated structural and geophysical modelling, in: Computer Methods in the Geosciences. Elsevier. Volume 15, pp. 303–324.

Judge, P. A., & Allmendinger, R. W. (2011). Assessing uncertainties in balanced cross sections. *Journal of Structural Geology*, *33*(4), 458-467.

Kempf, O., Matter, A., Burbank, D., Mange, M. (1999). Depositional and structural evolution of a foreland basin margin in a magnetostratigraphic framework: the Eastern Swiss Molasse basin. *International Journal of Earth Sciences* 88, 253–275.

Kuhlemann, J., Kempf, O. (2002). Post-Eocene evolution of the north alpine foreland basin and its response to alpine tectonics. *Sedimentary Geology* 152, 45–78.

Laubscher, H. P. (1961). Die fernschubhypothese der jurafaltung. *Eclogae Geologicae Helvetiae*, *54*(1), 222-282.

McElreath, R. (2018). Statistical rethinking: A Bayesian course with examples in R and Stan. Chapman and Hall/CRC.

Mann, C.J. (1993). Uncertainty in geology, in: Computers in geology—25 years of progress, pp. 241–254.

Metropolis, N., Rosenbluth, A.W., Rosenbluth, M.N., Teller, A.H., Teller, E. (1953). Equation of state calculations by fast computing machines. *Journal of Chemical Pyhsics* 21, 1087-1092.

Mock, S., von Hagke, C., Schlunegger, F., Dunkl, I., Herwegh, M. (2020). Long-wavelength late-Miocene thrusting in the north Alpine foreland: implications for late orogenic processes. *Solid Earth*, 11(5), 1823-1847.

Nelder, J. A., Mead, R. (1965). A simplex method for function minimization. *The Computer Journal*, 7, 308– 313.

Ortner, H., Aichholzer, S., Zerlauth, M., Pilser, R., Fügenschuh, B. (2015). Geometry, amount, and sequence of thrusting in the subalpine molasse of western Austria and southern Germany, European alps. *Tectonics* 34, 1–30.

Ortner, H., von Hagke, C., Sommaruga, A., Mock, S., Mosar, J., Hinsch, R., Beidinger, A. (2023). The northern deformation front of the European alps. *Geodynamics of the Alps-Collisional Processes*, *3*, 241-312.

Parks, V.M.B., McQuarrie, N. (2019). Kinematic, flexural, and thermal modelling in the central Andes: Unravelling age and signal of deformation, exhumation, and uplift. *Tectonophysics* 766, 302–325.

Pfiffner, O.A. (1986). Evolution of the north alpine foreland basin in the central alps. *Foreland basins*, 219–228.

Pollack, A., Cladouhos, T.T., Swyer, M., Horne, R., Mukerji, T. (2020). Stochastic inversion of gravity, magnetic, tracer, lithology, and fault data for geologically realistic structural models: Patua Geothermal Field case study. *Geothermics*, 95, 102129.

Reiners, P.W., Brandon, M.T. (2006). Using thermochronology to understand orogenic erosion. *Annu. Rev. Earth Planet. Sci*. 34, 419–466.

Reiners, P.W., Ehlers, T.A., Zeitler, P.K. (2005). Past, present, and future of thermochronology. *Reviews in Mineralogy and Geochemistry* 58, 1–18.

Sambridge, M., Mosegaard, K. (2002). Monte Carlo methods in geophysical inverse problems. *Reviews in geophysics*, 40, 3-1-3-29.

Schuller, V., Frisch, W., Herzog, U. (2015). Critical taper behaviour and out-of-sequence thrusting on orogenic wedges–an example of the eastern alpine molasse basin. *Terra Nova* 27, 231–237.

Squillacote, A.H., Ahrens, J., Law, C., Geveci, B., Moreland, K., King, B. (2007). The paraview guide. volume 366. Kitware Clifton Park, NY.

Stockli, D.F. (2005). Application of low-temperature thermochronometry to extensional tectonic settings. *Reviews in Mineralogy and Geochemistry* 58, 411–448.

Stuart, A. M. (2010). Inverse problems: a Bayesian perspective. *Acta numerica*, *19*, 451-559.

Thiele, S.T., Jessell, M.W., Lindsay, M., Wellmann, J.F., Pakyuz-Charrier, E. (2016). The topology of geology 2: Topological uncertainty. *Journal of Structural Geology* 91, 74–87.

Trümpy, R. (1960). Paleotectonic evolution of the central and western alps. *Geological Society of America Bulletin* 71, 843–907.

von Hagke, C., Cederbom, C., Oncken, O., Stöckli, D., Rahn, M., Schlunegger, F. (2012). Linking the Northern Alps with their foreland: The latest exhumation history resolved by low-temperature thermochronology. *Tectonics* 31.

von Hagke, C., Oncken, O., Ortner, H., Cederbom, C., Aichholzer, S. (2014). Late Miocene to present deformation and erosion of the central alps—evidence for steady state mountain building from thermokinematic data. *Tectonophysics* 632, 250–260.

Wagner, G., Reimer, G. (1972). Fission track tectonics: the tectonic interpretation of fission track apatite ages. *Earth and Planetary Science Letters* 14, 263–268.

Wellmann, J. F., Regenauer-Lieb, K. (2012). Uncertainties have a meaning: Information entropy as a quality measure for 3-D geological models. *Tectonophysics* 526, 207-216.

Wellmann, J.F., Horowitz, F.G., Schill, E., Regenauer-Lieb, K. (2010). Towards incorporating uncertainty of structural data in 3-D geological inversion. *Tectonophysics* 490, 141–151.

Wellmann, J.F., Thiele, S.T., Lindsay, M.D., Jessell, M.W. (2016). pynoddy 1.0: an experimental platform for automated 3-D kinematic and potential field modelling. *Geoscientific Model Development* 9, 1019–1035.

Wellmann, J.F., de la Varga, M., Murdie, R.E., Gessner, K., Jessell, M. (2018). Uncertainty estimation for a geological model of the Sandstone Greenstone belt, Western Australia – insights from integrated geological and geophysical inversion in a Bayesian inference framework. *Geological Society Special Publication* 453, 41-56.

Wolf, R., Farley, K., Silver, L. (1996). Helium diffusion and low-temperature thermochronometry of apatite. *Geochimica et Cosmochimica Acta* 60, 4231–4240.